

of temperatures, its applicability over a wide range of strain is however limited due to the use of split Hopkinson's pressure bar method (SHPB) that permits to achieve only a limited range of strains.

However, little literature on researches of tool wear based on thermodynamics constitutive mechanism is reported until now. The aim of this study is to deduce the thermodynamical constitutive equation of Incoloy 907 at high temperature, which is used to build an orthogonal FE model during high speed machining of Incoloy 907.

II. SIMULATION

The simulated cutting conditions are identical to those of the experiments performed on numerically controlled lathe utilizing a radial feed (Fig.1) at cutting speeds (v) of 300 m/min, 200 m/min, 150 m/min and 100 m/min, uncut chip thickness (b) of 0.15mm and width of cut (a_p) of 0.5mm. The cutting temperature (along the rake face in Fig.2) was measured using a infrared thermal imager and the cutting force was measured using a dynamometer. The chemical composition of workpiece material is shown in Table 1. The mechanical and physical properties of workpiece material and tool material are also presented in Table 2 and Table 3, respectively. The cutting tool geometry for WC CNMA432 consisted of a normal rake angle and a normal flank angle of 3° and 7° , respectively. The tool cutting edge angle is 90° , the tool cutting edge inclination angle is 0° . No cutting fluid was used in the tests.

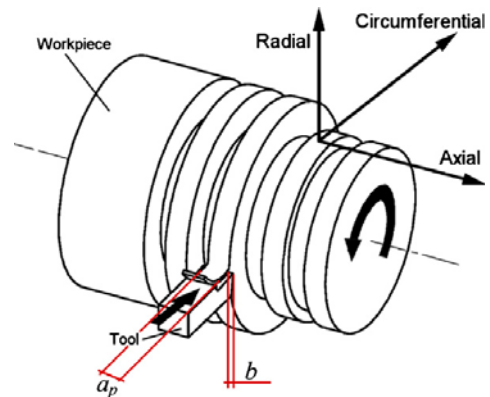


Figure 1. Configuration of the orthogonal cutting tests

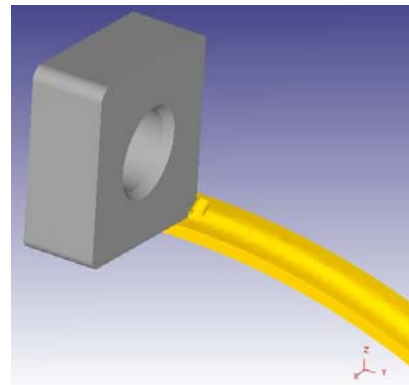


Figure 2. Tool and workpiece

TABLE I. CHEMICAL COMPOSITION OF INCOLOY 907^[17]

element	C	Ni	Co	Ti	Fe	Nb+Ta	Si
Component (wt.%)	≤0.06	35-40	12-16	1.3-1.8	其余	4.3-5.2	0.07-0.35

TABLE 2. MECHANICAL AND PHYSICAL PROPERTIES OF INCOLOY 907^[17]

Density	8280 kg/m ³
Ultimate tensile strength	1035MPa
Tensile yield strength	725MPa
Modulus of elasticity	160GPa
thermal conductivity	15.6W/(m.K)
Poisson's ratio	0.36
Heat capacity	431J/kg K

TABLE 3. MECHANICAL AND PHYSICAL PROPERTIES OF TOOL MATERIAL WC-Co^[18]

Density	14.5*10 ³ kg/m ³
Ultimate tensile strength	3000MPa
Modulus of elasticity	650GPa
thermal conductivity	58.9888W/(m.K)
Poisson's ratio	0.25
Heat capacity	15.0018 J/kg K

A. Numerical model of orthogonal machining

The commercial FEA software DEFORM-3D, a Lagrangian implicit code, is used to simulate the orthogonal cutting process of Incoloy 907. FEM model of the orthogonal cutting process is developed that the tool is no longer modeled as rigid.(Fig2). The workpiece is initially meshed with 8000 isoparametric quadrilateral elements, while the tool is modeled as non-rigid, and meshed and subdivided into 1000 elements(Fig3). A plane-strain coupled thermo-mechanical analysis is performed using orthogonal assumption.

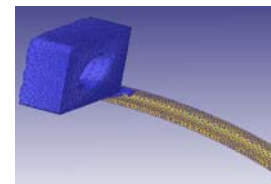


Figure 3. Meshed Tool and workpiece

B. Material modeling

To model the thermo-elas plastic behaviour of workpiece material Incoloy 907 and tool material WC-Co, the thermodynamics constitutive equation which is expressed as equation (1)^[19] is deduced and is used in this paper

$$\sigma = \left(B \varepsilon_p^n \right) \left(1 + B_1 T \left[\dot{\varepsilon}_p \right]^{\frac{1}{m}} - B_2 T e^{A \left(1 - \frac{T}{T_r} \right)} \right) + Y_a \quad (1)$$

Where A、B、B1、B2、n、m and Ya are seven constants associated with material.

Medeling of material constitutive behavior in a variety of applications is important. The conventional tension or compression tests are only applicable under low strain-rates(10⁻³-10⁻¹/s) and low temperature. In the machining processes, chip deformation, material constitutive relationships, and tool-chip friction are coupled together and affected each other.

According to principle of minimum energy dissipation, the occurrence of any process will happen on the least energy-consuming way, so as the plastic deformation of cutting process. The thermodynamics constitutive equation is deduced according to principle of minimum energy dissipation, which has taken into account coupling in the derivation, so the application of thermodynamics constitutive equation in simulation will be a new exploration in machining.

1) Determination of parameters

a) Doing orthogonal cutting experiments to collect cutting force date Fz、Fy, and to measure the thickness of chip.

b) calculating the ratio of the actual cutting force obtained from experiment and the ratio of the actual chip deformation coefficient obtained from experiment

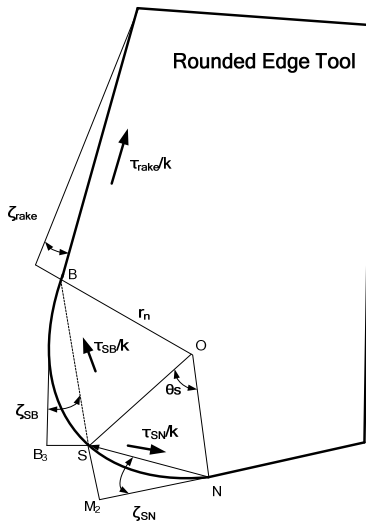


Figure4. Rounded edge tool

c) calculating the ratio of the predicted cutting force and the ratio of the predicted chip deformation coefficient Cross-sectional of rounded edge tool is as follows(Fig.4)

τ_{rake}/k is the ratio of shear stress and flow stress of workpiece materials in the rake face, ζ_{rake} is an angle associated with the above ratio, τ_{SB}/k is the ratio of shear stress along the tool arc cutting edge SB and flow stress of workpiece materials in the rake face, ζ_{SB} is an angle associated with the above ratio; τ_{SN}/k is the ratio of shear stress along the tool arc cutting edge SN and flow stress of workpiece materials in the rake face, ζ_{SN} is an angle associated with the above ratio; θ_s is central angle of residual layer of the formation of point S with the tool edge end point N.

i Assuming $\tau_{rake}/k = \tau_{SB}/k = \tau_{SN}/k = 0.5$ and $\theta_s = 10^\circ$

ii Calculating the angle ζ_{SB} 、 ζ_{SN} and ζ_{rake}

$$\zeta_{SB} = \left[\cos^{-1} \left(\tau_{SB} / k \right) \right] / 2 \quad (2)$$

$$\zeta_{SN} = \left[\cos^{-1} \left(\tau_{SN} / k \right) \right] / 2 \quad (3)$$

$$\zeta_{rake} = \left[\cos^{-1} \left(\tau_{rake} / k \right) \right] / 2 \quad (4)$$

iii Calculating the theoretical thickness of chip

$$h_{ch} = \sqrt{2} \cos \left(\pi / 4 - \zeta_{rake} \right) \left(BH \cos \zeta_{rake} + SB \cos \zeta_{SB} \right) \quad (5)$$

Where

$$BH = \frac{hc + \sqrt{2} \left(\Delta S + SB \cos \zeta_{SB} \right) \sin \delta - r_n \left(1 + \sin \gamma_0 \right)}{\left(\cos \zeta_{rake} + \sin \zeta_{rake} \right) \sin \left(\gamma_0 + \zeta_{rake} \right)} \quad (6)$$

$$SB = 2r_n \sin \left(\frac{\pi}{4} + \frac{\gamma_0}{2} - \frac{\theta_s}{2} \right) \quad (7)$$

$$\Delta S = \sqrt{2} r_n \sqrt{1 - \frac{\tau_{SN}}{k}} \sin \left(\frac{\theta_s}{2} \right) \quad (8)$$

$$\delta = \pi / 4 - \gamma_0 - \zeta_{rake} \quad (9)$$

iv Calculating the shear angle φ , $\varphi = \gamma_0 + \zeta_{rake}$

F. Calculating the ratio of the predicted cutting force and the ratio of the predicted chip deformation coefficient

$$\left(\frac{F_z}{F_y} \right)_{pr} = \frac{1}{\tan \left(\operatorname{atan} \left(\frac{\tau_{rake}}{k} \right) - \gamma_0 \right)} \quad (10)$$

$$\zeta_{pr} = \frac{h_{ch}}{h_c} \quad (11)$$

If the predicted value and the actual value can meet with the following relationship, then export the flow stress strain strain rate and temperature ; if not, then re-assume the value of $\tau_{rake}/k=\tau_{SB}/k=\tau_{SN}/k$ and θ_s , till meeting the following relationship.

$$\left[\left(\frac{F_z}{F_y} \right)_{pr} - \left(\frac{F_z}{F_y} \right)_{ex} \right]^2 + \left[\left(\frac{h_{ch}}{h_c} \right)_{pr} - \left(\frac{h_{ch}}{h_c} \right)_{ex} \right]^2 \leq 10^{-12} \quad (12)$$

d) Calculating the flow stress strain ,strain rate and temperature with the following equations.

$$\sigma = k = \frac{F_z}{A} = \frac{F_z}{h_c w} \quad (13)$$

$$\gamma = \frac{\cos \gamma_0}{2 \sin \phi \cos(\phi - \gamma_0)} \quad (14)$$

$$\dot{\gamma}_{ave} = \frac{v_s}{\Delta S} \quad (15)$$

$$v_s = \frac{\cos \gamma_0}{\cos(\phi - \gamma_0)} v_c \quad (16)$$

$$T = T_w + \eta \left[\frac{1 - \beta}{\rho_s S} \frac{k \cos \gamma_0}{\sin \phi \cos(\phi - \gamma_0)} \right] \quad (17)$$

The flow chat of calculating the four parameters is as follows(Fig.5).

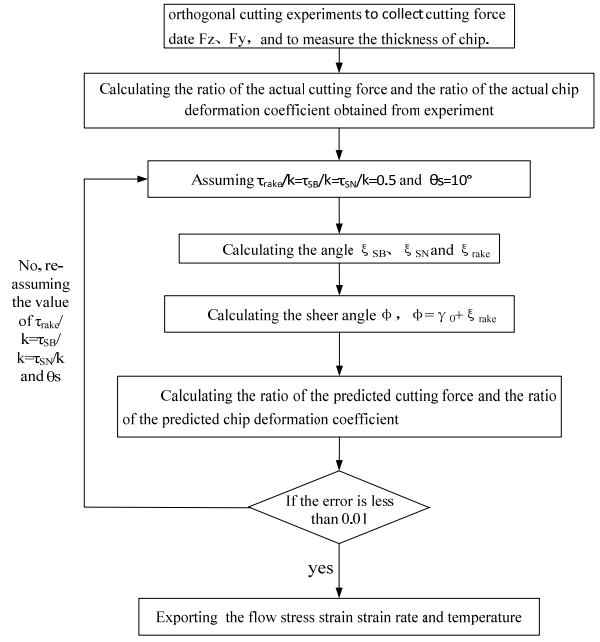


Figure 5. Flow chat

2) Non-linear fitting of thermodynamics constitutive equation

The thermodynamic constitutive equations were non-linearly fitted with the least-squares method according to the four parameters (flow stress ,strain ,strain rate and temperature), and the material coefficients were simultaneously determined which make the norm of the residual sum of squares between the calculated modified flow stress value and the actual value obtained by experiments be less 0.01. The fitting parameters of high-temperature alloy Incoloy 907 were as follows in Tab.4

TABLE4. MATERIAL COEFFICIENTS OF INCOLOY 907

B1	B2	B	A	n	m	Ya
0.1012	-0.1212	1.0903	-0.9011	3.5514	0.0875	977.0904

The ultimate thermodynamical constitutive equations for workpiece material Incoloy 907was obtained as:

$$\sigma = (1.0903 \varepsilon_p^{3.5514}) \left(1 + 0.1012 T [\dot{\varepsilon}_p]^{0.0875} + 0.1212 T e^{-0.9011 \left(1 - \frac{T}{T_i} \right)} \right) + 977.0904 \quad (18)$$

From the research of Hayakawa K^[20], the strain and stress at normal temperature of tool material WC-Co were as follows in Tab.5.

TABLE5. MATERIAL STRAIN AND STRESS DATA OF TOOL MATERIAL WC-Co

strain	0	0.005	0.01	0.015	0.02
stress (MPa)	0	2000	2700	2800	3000

The ultimate thermodynamical constitutive equations for

tool material WC-CO was obtained as:

$$\sigma = (2.029 e^{0.2735}) \left(1 + 0.0001 T [\dot{\varepsilon}_p]^{0.0001} - 0.6906 T e^{0.3047 \left(1 - \frac{T}{1372} \right)} \right) + 2.1 \quad (19)$$

To validate the orthogonal cutting model, the predicted and experimentally measured cutting temperature and Cutting force were compared and their differences were discussed.

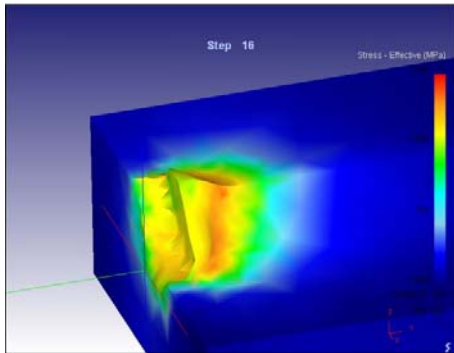
C. Experimental verification

Orthogonal cutting tests were performed on a numerically controlled lathe equipped with a specially designed experimental set-up. In measuring the cutting force components (tangential force and the thrust force) a Kistler-type SDC CSM19 three-component piezoelectric dynamometer was used. The tangential force component was measured in the direction of the primary motion and the thrust force component in the direction of feed motion. The experimental value were shown in Tab.6.

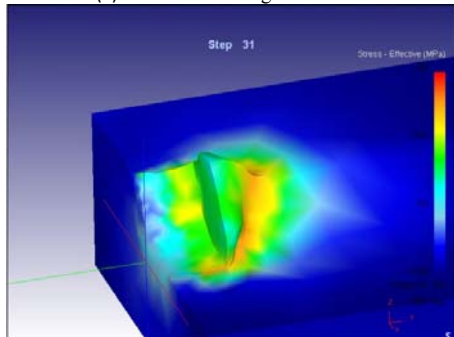
D. Simulation results and discussion

1) Flow stress and equivalent strain

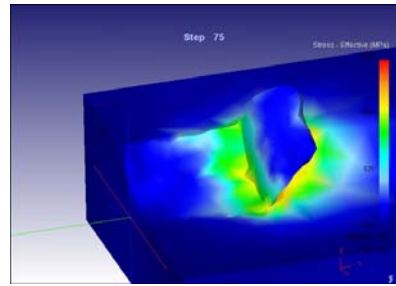
The predicted flow stress of workpiece and chip when two-dimensional orthogonal cutting INCOLOY when cutting speed was 100m/min were shown in Fig.6. It can be seen from Fig.7 that the flow stress of workpiece and chip decreased smoothly when the tool had just cut into the workpiece, then the flow stress of workpiece fluctuated within a certain range when steady-state cutting whose reasons were as follows: firstly, the increasing temperature of the shear zone would cause the thermal softening of workpiece material which would make the material flow stress reduction, simultaneously, the decreased flow stress would make the heat reduction which would make the uncut material hardened and would cause the flow stress increased. It can also be seen from Fig.7 that the flow stress in the chip was gradually released with the running-out of the chip from the rake face of the tool, and the flow stress in the workpiece only existed near the cutting region while away from the cutting region the regional stress was small.



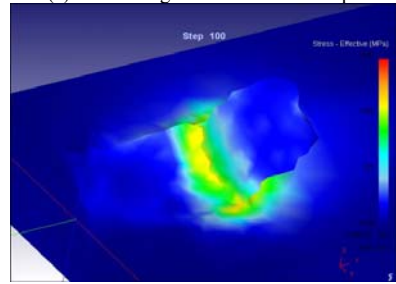
(a) The initial cutting stress field



(b) The cutting stress field of 31 steps

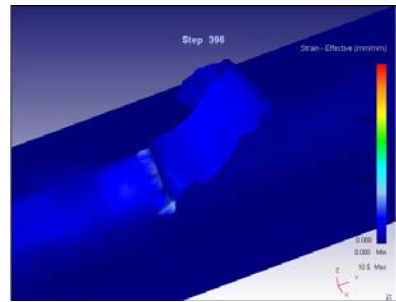


(c) The cutting stress field of 75 steps

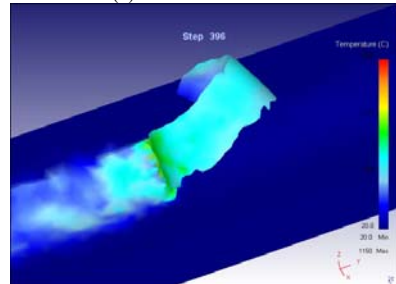


(d) The cutting stress field of 100 steps

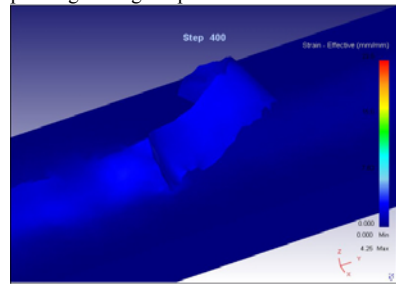
Figure6. Distribution of equivalent stress



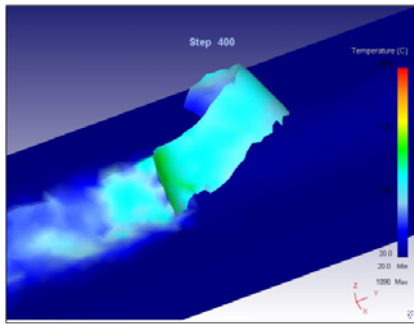
(a) Non-uniform strain



(b) The corresponding cutting temperature field for the non-uniform Strain



(c) Uniform strain

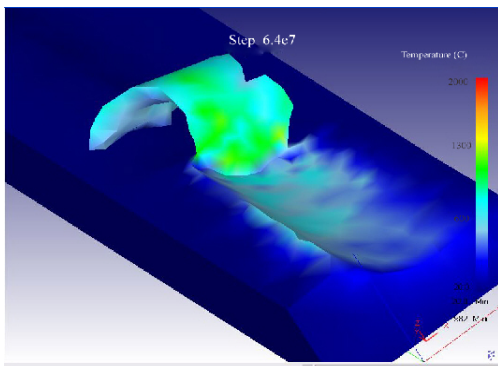


(d) The corresponding cutting temperature field for the uniform strain
Figure7. Distribution of equivalent strain

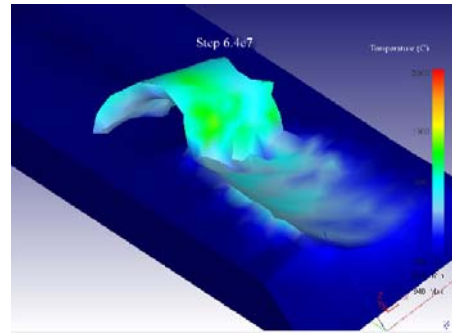
The predicted equivalent strain of workpiece and chip when two-dimensional orthogonal cutting Incoloy 907 when cutting speed was 100m/min were shown in Fig.7(a)and(c).The corresponding cutting temperature field were shown in Fig.7(b)and(d). It can be seen from Fig.8 that the maximum equivalent strain distributed in the area where the chip was about to leave the rake face of the tool. When steady-state cutting, the strain of workpiece was uniform, as the cutting process progressed the strain became uneven, and the fluctuations of strain were taken place in the workpiece whose fluctuations in frequency was lower than the fluctuations of stress. The reasons were as follows: the dynamic recrystallization of the materials would cause the stress softening of the material as the increasing of the cutting temperature, simultaneously , changes in microstructure took place with the deformation. The small differences of microstructure in the spatial distribution could cause a large difference of macroscopic stress and strain for the non-linear relationship between the microstructure changes and the macro-deformation , samely, the macro-inhomogeneity of deformation could also cause more uniform microstructure which would make the strain fluctuation.

2) Cutting temperature

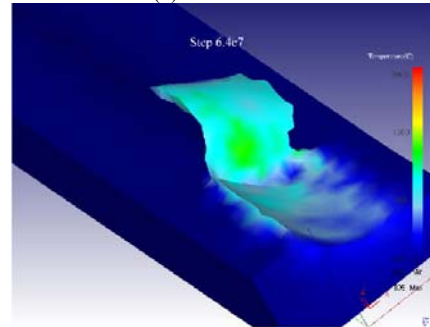
The predicted temperature at different cutting speed were showed in Fig.8. It can be obviously seen that the predicted temperature increased with the increasing of the cutting speed. The predicted temperature reached to 1290 °C when the cutting speed was 300m/min while the cutting speed was 100m/min, the predicted temperature only reached to 810 °C .



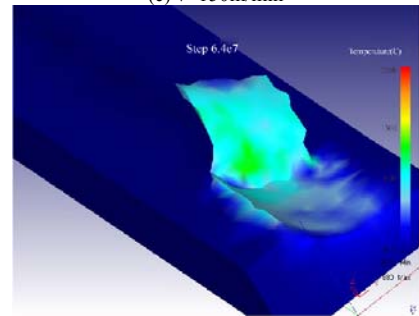
(a) v=300m/min



(b) v=200m/min



(c) v=150m/min

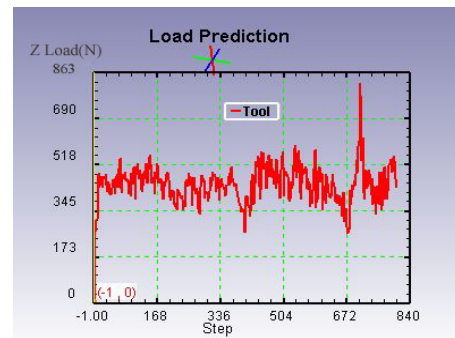


(d) v=100m/min

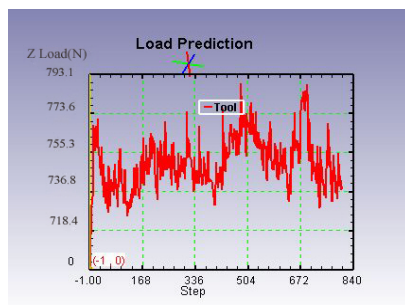
Figure8. Predicted temperature

3) Cutting force

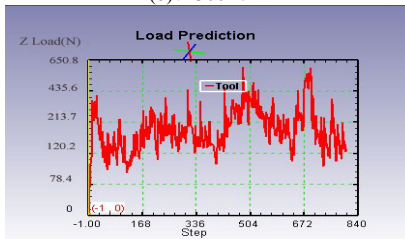
The predicted cutting force at different cutting speed were showed in Fig.9.



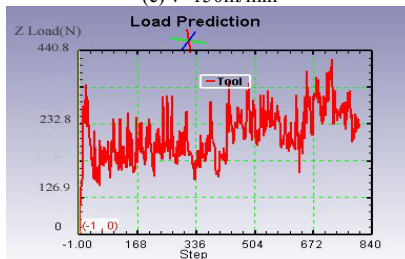
(a) v=200m/min



(b)v=300m/min



(c) v=150m/min



(d)v=100m/min

Figure9. Predicted cutting force

In order to verify the correctness of the obtained finite element model, the experimental value and predicted value were compared which were shown in Tab.6. The results showed that the relative error between the experimental value and predicted value was less than 10% which proved the correctness of the obtained model for the model was built under some certain assumption. This result permits to assess that the assumption of the T-C-Q model used in the present study appears to be reasonable. Tab.6 gives the experimental value and predicted value .

TABLE 6. THE EXPERIMENTAL VALUE AND PREDICTED VALUE (THE DISTANCE IS0.05MM BETWEEN TOOL RAKE FACE AND CHIP EDGE)

Cutting speed (m/min)	100	150	200	300
Predicted cutting force/N	431.5	645.41	860.24	720
Experimental cutting force/N	422.23	597	789	661
Relative error	2.2%	8.3%	9.5%	8.8%
Predicted temperatue/°C	810	1010	1220	1290
Experimental temperatue /°C	637	957	1128	1230
Relative error	8.7%	5.5%	8.1%	4.87

III. CONCLUSION

A finite element analysis (FEA) of machining for Incoloy907 is presented. In particular, the thermodynamical constitutive equation (T-C-E) in FEA is applied for both work piece material and tool material. Research results indicated that a reasonable prediction of temperature and cutting force are obtained when using model T-C-E in high speed machining. These evidences permit to establish that good numerical results can be obtained when simulating cutting conditions similar to those characterize material constitutive law. Therefore, it can be concluded that the T-C-E model in this paper can be employed to study the orthogonal process of Incoloy907 and to predict the reality of the temperature and cutting force with satisfactory accuracy.

ACKNOWLEDGMENTS

The author gratefully acknowledges Prof. Huanjie Zhang at the Binzhou Bohai Piston Limited Company for providing the experimental results for this research, and also acknowledges the Binzhou Polytechnic Natural Science Foundation(2010xykt03).

CONFERENCES

- [1] E. O. Ezugwu. Journal of Materials Processing Technology.185 (2007):60-71.
- [2] F.C. Campbell. Manufacturing Technology for Aerospace Structural Materials. (2006) :211-272.
- [3] RL Kennedy, RM Forbes Jones, RM Davis, MG Benz and, WT Carter. Vacuum47(1996): 819-824.
- [4] J.S. Wan, Z.F. Yue. Materials Science and Engineering: A.392(2005): 145-149
- [5] J. W. Brooks. Materials & Design.21(2000): 297-303.
- [6] T. Kitashima, H. Harada. Acta Materialia.57(2009): 2020-2028.
- [7] T. Link, S. Zabler, A. Epishin, A. Haibel, M. Bansal, X. Thibault r. Materials Science and Engineering: A.425(2006): 47-54.
- [8] Florian Pyczak, Steffen Neumeier, Mathias Göken. Materials Science and Engineering: A.510-511(2009): 295-300.
- [9] E. O. Ezugwu, Z. M. Wang. Journal of Materials Processing Technology.68(1997):262-274.
- [10] Domenico Umbrello. Journal of materials processing technology. 196(2008):79-87.
- [11] Songwon Seoa, Oakkey Minb, Hyunmo Yang. International Journal of Impact Engineering 31(2005):735-754.
- [12] D.Rittel , Z.G. Wang. Mechanics of Materials. 40(2008):629-635.
- [13] Woei-Shyan Lee, Chi-Feng Lin. Journal of Materials Processing Technology .75(1998):127-136.
- [14] Y.Q. Wang, G. Sayre. Surface and Coatings Technology.203(2008): 256-263.
- [15] A.K. Koul, F.B. Pickering. Scripta Metallurgica.16(1982): 119-124
- [16] S. Miller. Interdisciplinary Science Review.21(1996): 117-129.
- [17] China Aeronautical Materials Handbook prepared by the Commission. China Aeronautical Materials Handbook (Volume 2) High-temperature deformation alloy High-temperature casting alloy[M].Beijing: Standards Press of China.
- [18] D. Umbrelloa, R. M Saoubib, J.C.Outeiro . International Journal of Machine Tools & Manufacture .47(2007):462-470.
- [19] George Z. Voyiadjis , Amin H. Almasri. Mechanics of Materials 40(2008):549-563.
- [20] M.Jr.Vaz. Journal of Brazilian Society of Mechanical Science. 22(2000):179-188.